Inorganic Chemistry

pubs.acs.org/IC

Article

Efficient Separation of Trace SO_2 from $SO_2/CO_2/N_2$ Mixtures in a Th-Based MOF

Wenhui Zhang,[§] Wansheng Jia,[§] Jie Qin, Lan Chen, Youyuan Ran, Rajamani Krishna, Li Wang,* and Feng Luo*

Cite This: *Inorg. Chem.* 2022, 61, 11879−11885

Read Online

ACCESS | Metrics & More | Article Recommendations | Supporting Information

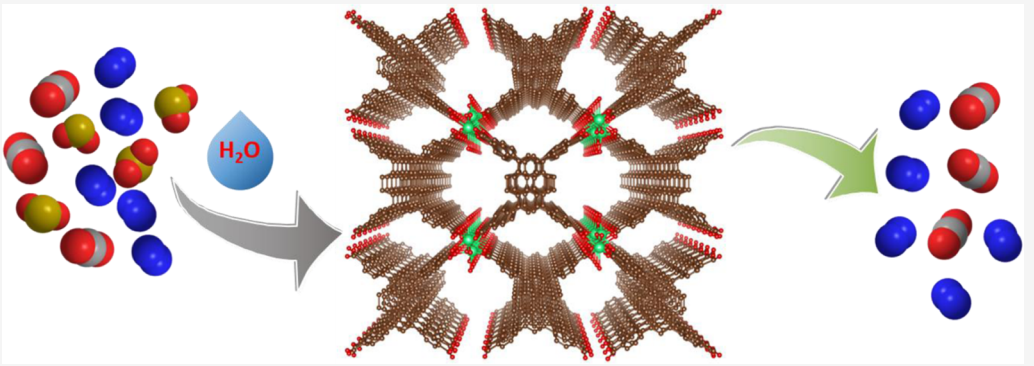

ABSTRACT: The emission of sulfur dioxide (SO_2) from flue gases is harmful since trace SO_2 impairs human health and the natural environment. Therefore, developing new metal organic frameworks (MOFs) to capture this toxic molecule is of great importance in flue gas desulfurization. In this work, we synthesized a new MOF, namely, **ECUT-Th-60**, which consists of two distinct channels (3.0 Å × 4.1 Å and 2.3 Å × 4.8 Å). It shows SO_2 uptakes of around 2.5 mmol/g at 0.1 kPa and 3.35 mmol/g at 1 bar, which are higher than those of CO_2 and N_2 under identical conditions. Both simulated and experimental breakthrough tests proved that **ECUT-Th-60** can separate trace SO_2 from SO_2/CO_2 mixtures. Impressively, complete separation of SO_2 from $SO_2/CO_2/N_2$ mixtures under both dry and humid conditions was also proved in **ECUT-Th-60**, predicting its potential application in flue gas desulfurization.

INTRODUCTION

Sulfur dioxide (SO_2), induced by the massive combustion of fossil fuels, is harmful to human health (i.e., respiratory disease) and the environment (i.e., acid rain) due to its high corrosivity.[1−7] It has already been listed as one of the most hazardous gases by the World Health Organization (WHO).[8,9] As a consequence, various strategies have been investigated to decrease SO_2 emissions. On the other hand, if SO_2 was gathered and purified, it could be utilized in the industry for producing sulfuric acid.[10] At present, established desulfurization technologies such as using sodium hydroxide, ammonia scrubbing, or using limestone-gypsum as an alkaline absorbent are in use.[11−14] However, all of these absorbents suffer from shortcomings such as regeneration and recovery issues, hard to produce new byproducts, and so on.[15] Importantly, only approximately 95% of SO_2 can be removed using these methods. The residual trace amount of SO_2 remains in the flue gas.[16−18] As we know, even trace SO_2 could irreversibly influence the purification processes of other flue gases such as CO_2 or inactivate the adsorbents in the industry.[19−23] Therefore, searching for a new effective adsorption technology to achieve deep flue gas desulfurization (FGD) has evoked widespread attention from the aspect of sustainable development.

As an alternative, hybrid porous materials have been proposed for SO_2 capture very recently. Metal organic frameworks (MOFs), assembled by metal cation/clusters and organic linkers, have been considered promising candidates for gas separation due to their easily tunable structure required to guarantee shape or size selectivity. At present, many reported MOFs have been applied for the separation of binary components such as C_3H_8/C_3H_6,[24,25] C_3H_6/C_2H_4,[26] C_3H_4/C_3H_6,[27,28] C_2H_2/C_2H_4,[29,30] C_2H_4/C_2H_6,[31,32] and CO_2/C_2H_2[33,34] and ternary components such as $CH_4/C_2H_6/C_3H_8$,[35] and $C_2H_4/C_2H_2/C_2H_6$.[36] However, compared with

Received: May 11, 2022
Published: July 20, 2022

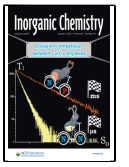

https://doi.org/10.1021/acs.inorgchem.2c01634
Inorg. Chem. 2022, 61, 11879−11885

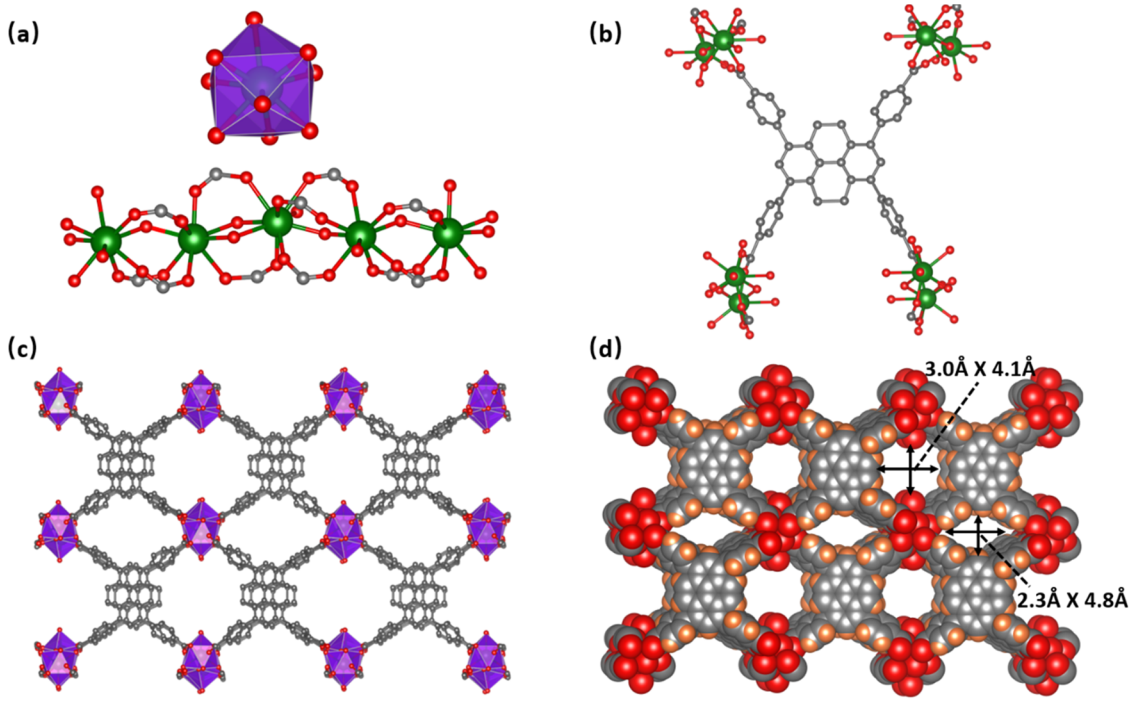

Figure 1. (a) Coordination environment of Th^{4+}. (b) Coordination mode of the TBAPy ligand. (c) Framework structure of **ECUT-Th-60** along the [001] direction. (d) Corresponding space-filling models and the size of the two different channels along the [001] direction. Gray, C; red, O; green, Th; and orange, H.

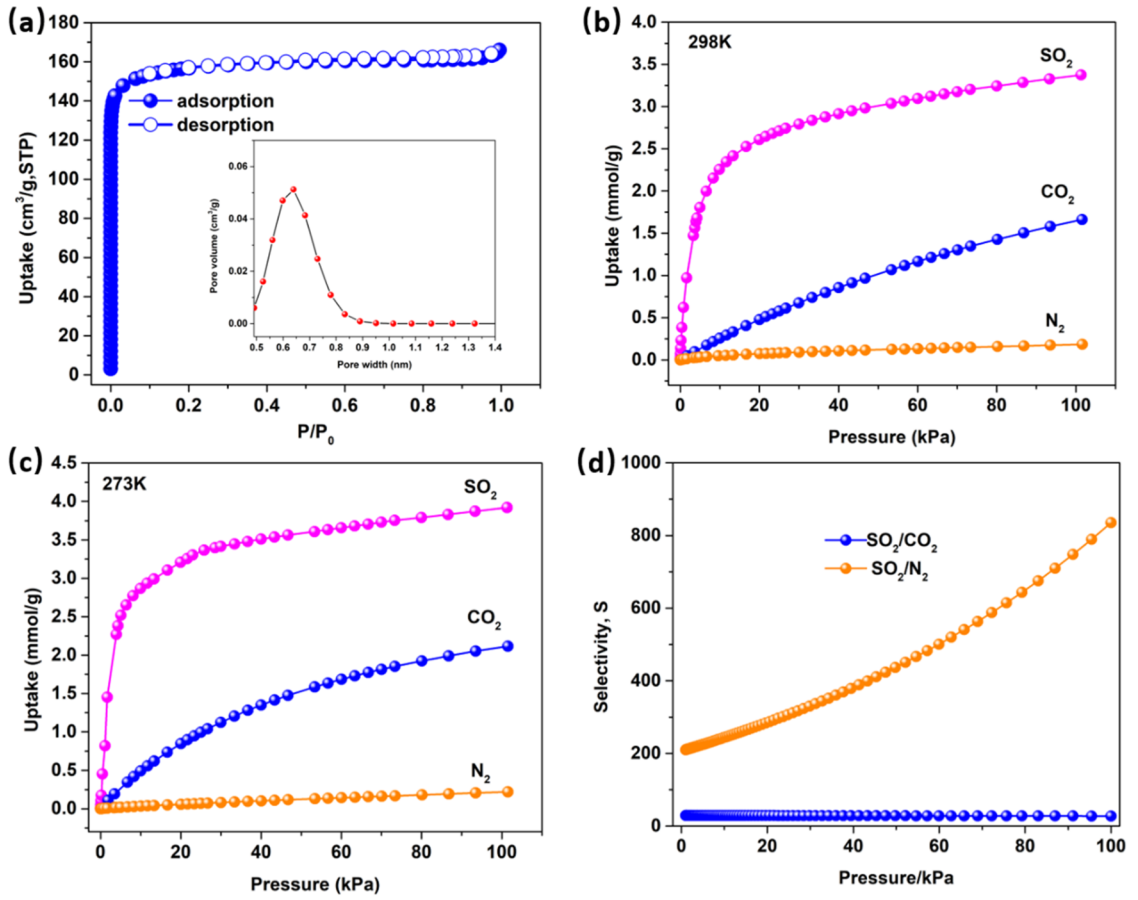

Figure 2. (a) N_2 adsorption and desorption isotherms of **ECUT-Th-60** at 77 K. (b) and (c) Adsorption isotherms for SO_2, CO_2, and N_2 in **ECUT-Th-60** at different temperatures. (d) IAST selectivity of SO_2/CO_2 (1:99) and SO_2/N_2 (1:99) in **ECUT-Th-60**.

https://doi.org/10.1021/acs.inorgchem.2c01634
Inorg. Chem. 2022, 61, 11879−11885

other gas sorption and separation methods, the number of MOFs reported for SO_2 adsorption are small because of its corrosive and destructive effect on the structure of MOFs.[37] Especially under humid conditions, since SO_2 can easily lead to the generation of sulfite or sulfuric acid under water or oxygen conditions, suitable MOFs for SO_2 separation are scarcely reported. For example, MOF-177 has a high SO_2 uptake of 25.7 mmol/g at 298 K, but its crystallinity is changed after SO_2 adsorption, indicating its chemical instability and unsuitability for SO_2 separation.[38] Other reported MOFs such as MIL-125(Ti)-NH_2 and MFM-202a also suffered from this problem.[39,40] As we know, the flue gas mixture usually consists of N_2 or CO_2 with a small part of SO_2 (50−3000 ppm). Therefore, developing new MOFs with high adsorption capacity and selectivity of SO_2 over N_2 and CO_2 and high stability under humid conditions is of great significance. In addition, the reversibility and energy-efficient recovery for MOFs should be considered as well.

In this work, we reported a novel MOF, which has a higher SO_2 uptake than those of CO_2 and N_2 under identical conditions. Both breakthrough simulations and experiments were conducted to illustrate the separation performance of **ECUT-Th-60** with a simulated flue gas ($SO_2/CO_2/N_2$ mixtures) under dry and humid conditions.

RESULTS AND DISCUSSION

The crystals of **ECUT-Th-60** were synthesized by the solvothermal method (Figure S1). $Th(NO_3)_4$ and H_4L were dissolved in a DMF solution at 110 °C. The synthesis process is detailed in the Supporting Information. The structure was determined by single-crystal X-ray diffraction. **ECUT-Th-60** crystallized in the monoclinic space group *C*2/*m*. Two independent thorium metal ions (Th1 and Th2) were coordinated to nine oxygen atoms with a distance from 2.33 to 2.61 Å (Figure 1a), which is in the normal range.[41,42] The adjacent thorium ions were quadruply bridged by oxygen, generating an infinite 1D metal chain. Each TBAPy ligand was coordinated to eight thorium ions due to the four carboxylate groups, where the linking pattern was μ^2−η^2: η^1 (Figure 1b). The packing diagram of **ECUT-Th-60** gave two crystallographically distinct channels (3.0 Å × 4.1 Å and 2.3 Å × 4.8 Å, considering the van der Waals radii of atoms) along the [001] direction (Figure 1c,d). It is worth noting that the size of the channels was comparable with the molecular size of SO_2 (2.9 Å × 3.4 Å × 4.8 Å),[43,44] suggesting that **ECUT-Th-60** might result in a reasonable capture ability of SO_2.

To verify the conjecture from the structure of **ECUT-Th-60**, bulk crystals were synthesized for further research. The matching powder X-ray diffraction (PXRD) patterns of simulated and experimental **ECUT-Th-60** indicated that no other phase existed, indicating the pure phase in bulk **ECUT-Th-60** (Figures S2 and S3). The thermal stability of **ECUT-Th-60** was investigated by thermogravimetric analysis (Figure S4). The initial mass losses up to 250 °C can be attributed to the guest molecules such as DMF in the channels. After 450 °C, a significant mass loss occurred corresponding to the collapse of the framework of **ECUT-Th-60**. Upon immersing in methanol for 3 days, the TG curve showed that methanol can be eliminated at around 150 °C. Therefore, the activated **ECUT-Th-60** was prepared at 150 °C under vacuum conditions. Both **ECUT-Th-60** after being immersed in methanol and **ECUT-Th-60a** retain their framework as evidenced by PXRD (Figure S3).

To examine the porosity, the N_2 adsorption−desorption behavior of **ECUT-Th-60** was investigated at 77 K. As shown in Figure 2a, a sharp increase was observed at low pressure for **ECUT-Th-60**, which presented a typical I adsorption with an uptake capacity of N_2 of up to 170 cm^3/g at 1 bar. The Brunauer−Emmett−Teller (BET) surface area was calculated to be 472 m^2/g.

Permanent porosity motivated us to investigate the adsorptive performance of **ECUT-Th-60**. Single-component isotherms of SO_2 were measured on **ECUT-Th-60** at 273 and 298 K, respectively. The saturation adsorption capacity of SO_2 reached 3.35 and 4.0 mmol/g at 298 and 273 K under 1 bar, respectively, which exceeded those of other materials such as commercial porous carbon (3.3 mmol/g), MOF-74 (3.03 mmol/g), SIFSIX-3-Ni (2.74 mmol/g), SIFSIX-3-Zn (2.10 mmol/g), and CPL-1 (2 mmol/g).[4,45,46] At low pressure of 0.1 bar, the uptake of SO_2 achieved was already 2.5 mmol/g, about 75% of the total uptake at 298 K and 1 bar. As we know, CO_2 is the main competitor for SO_2 removal. In addition, a higher selectivity of SO_2 over N_2 is also necessary. Therefore, the adsorption of CO_2 and N_2 at 298 and 273 K was also performed. Although SO_2 and CO_2 are both acidic, the CO_2 isotherms on **ECUT-Th-60** were completely different from the SO_2 isotherms at either 298 or 273 K. Obviously, the adsorption isotherms of SO_2 are steeper than those of CO_2 and N_2. The uptake capacity of CO_2 was only 1.7 mmol/g under 1 bar and 0.25 mmol/g under 0.1 bar at 298 K, which was significantly lower than that of SO_2 under identical conditions. A similar observation was also found for N_2 adsorption. The adsorption capacity of N_2 was only 0.18 mmol/g under 1 bar and 0.04 mmol/g under 0.1 bar at 298 K, which can be considered negligible compared with the adsorption capacity of SO_2. Such a significant difference in uptake capacity provided the great potential of separating SO_2 over CO_2 and N_2 on **ECUT-Th-60**.

The isosteric heats of adsorption (Q_{st}) of SO_2 and CO_2 were calculated based on adsorption isotherms at 273 and 298 K using the Clausius−Clapeyron equation.[47,48] The Q_{st} value of SO_2 increased from 14 to 57 kJ/mol over the whole range, whereas the value remained almost constant for CO_2 (17.8 kJ/mol) (Figure S5). The calculated Q_{st} for SO_2 at full loading is higher than those of other MOFs such as ELM-12 (41.6 kJ/mol),[13] MFM-300 (In) (39.6 kJ/mol),[37] SIFSIX-1-Cu (36.1 kJ/mol), and SIFSIX-3-Zn (45.2 kJ/mol).[45] The high Q_{st} of SO_2 indicated a strong affinity of the **ECUT-Th-60** framework toward SO_2.

To evaluate the separation property of **ECUT-Th-60**, Henry's constant of SO_2 and CO_2 and Henry's selectivity were also calculated based on the adsorption data at low pressure.[49] Henry's constant was calculated to be 34.28 (mmol/g)/bar for SO_2 and 2.56 (mmol/g)/bar for CO_2 (Figures S6 and S7). Henry's selectivity for SO_2/CO_2 was 13. Furthermore, the adsorption selectivity was also determined using ideal adsorbed solution theory (IAST) calculations, which are also very useful in predicting gas separation. The IAST selectivity of **ECUT-Th-60** for mixed gases of SO_2/CO_2 (1/99 v/v) and SO_2/N_2 (1/99 v/v) was calculated after fitting isotherms at 298 K to the dual-site Langmuir−Freundlich equation. The fitting parameters are shown in Table S1. As shown in Figure 2d, the selectivity reached 27 for SO_2/CO_2 at 298 K and 1 bar, which is lower than those of MFM-300 (In) (50),[37] SIFSIX-1-Cu (70.7), and SIFSIX-2-Cu-I (87.1).[45] However, it is still higher than those

https://doi.org/10.1021/acs.inorgchem.2c01634
Inorg. Chem. 2022, 61, 11879−11885

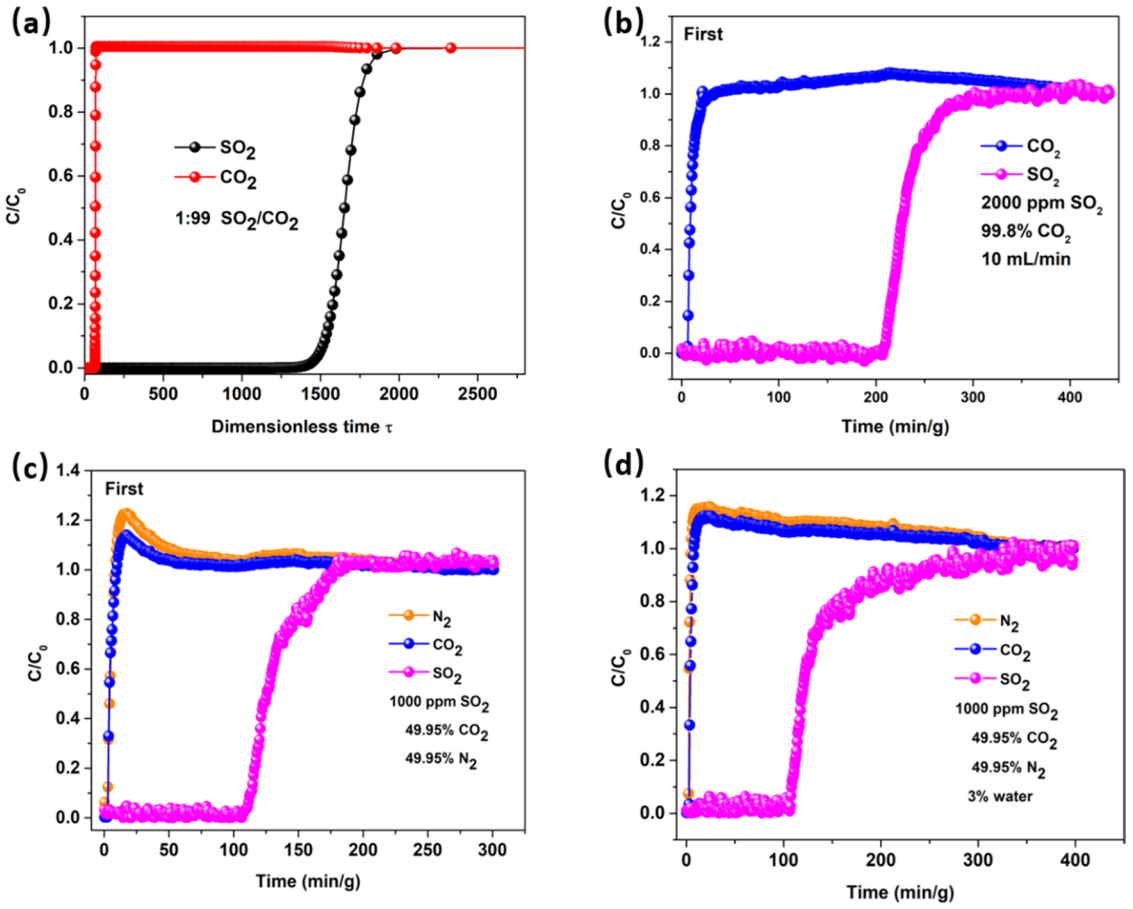

Figure 3. (a) Simulated breakthrough for the 1:99 (v/v) SO_2/CO_2 mixture on **ECUT-Th-60**. (b) Experimental breakthrough for the SO_2/CO_2 mixture at 298 K on **ECUT-Th-60**. (c) and (d) Experimental breakthrough for the SO_2/CO_2 /N_2 mixture without and with 3% water. The flow rate is 10 mL/min.

of the benchmark cs-carbons (~20), BC-4-650 (21), and BC-5-650 (22).[50,51] The selectivity for SO_2/N_2 was up to 835 at 298 K and 1 bar. All of these outstanding selectivities strongly suggested the preferable adsorption of SO_2 over CO_2 and N_2 on **ECUT-Th-60**.

Motivated by the different uptakes between SO_2, CO_2, and N_2 in **ECUT-Th-60**, we first evaluated the separation ability by a simulated breakthrough (Figure 3a). Obviously, the long separation time of about $\Delta\tau$ = 1400 for SO_2 separation indicated that **ECUT-Th-60** might be the potential material in SO_2/CO_2 separation. To further investigate the separation ability of **ECUT-Th-60** in real conditions, dynamic breakthrough experiments were carried out. First, a SO_2/CO_2 mixture containing 2000 ppm of SO_2 was introduced into the column packed with **ECUT-Th-60a**. Clearly, CO_2 started to break through the column rapidly after 6 min/g, while the SO_2 breakthrough occurred after 206 min/g. This result further confirmed the outstanding SO_2 separation ability of **ECUT-Th-60**. Given that a stable cycling performance and easy regeneration are extremely important in the industry, the breakthrough experiments were tested in duplicate. As shown in Figure S8, no significant decrease in the retention time for SO_2 was observed, indicating that the stability of **ECUT-Th-60** was well retained. Then, we used another ternary mixture of $SO_2/CO_2/N_2$ containing 1000 ppm of SO_2 to mimic the flue gas. As shown in Figure 3c, CO_2 and N_2 were rapidly eluted after 3 min/g, followed by SO_2 after 105 min/g. The recycling use was further confirmed by another cycling test (Figure S9).

The breakthrough experiments proved that **ECUT-Th-60** has potential application in the removal of SO_2 from dry gas mixtures. Considering that the primary content of flue gas is CO_2, N_2, and water vapor, the separation ability of our MOF under humid conditions (3% water) was also investigated. Impressively, the retention time for SO_2 achieved was still 105 min/g, which by far exceeded those of CO_2 and N_2 (Figure 3d). This result is comparable with the breakthrough experiments under dry conditions, which further confirmed the superior SO_2 separation ability of **ECUT-Th-60** even under humid conditions.

CONCLUSIONS

In summary, this work reported a new microporous MOF, **ECUT-Th-60**, as the potential SO_2 adsorbent. Single-component adsorption isotherms of SO_2, CO_2, and N_2 revealed a higher uptake of SO_2 than CO_2 and N_2. Experimental breakthrough tests further confirmed that SO_2 could be separated from SO_2/CO_2 or $SO_2/CO_2/N_2$ mixtures with a ppm level. The good recycling ability of **ECUT-Th-60** indicated that it could be applied in the industry considering its cost and practicability.

ASSOCIATED CONTENT

Supporting Information

The Supporting Information is available free of charge at https://pubs.acs.org/doi/10.1021/acs.inorgchem.2c01634.

https://doi.org/10.1021/acs.inorgchem.2c01634
Inorg. Chem. 2022, 61, 11879−11885

Details of synthesis and instruments and other characterizations such as PXRD, TG, and experimental breakthrough experiments (PDF)

Accession Codes

CCDC 2166695 contains the supplementary crystallographic data for this paper. These data can be obtained free of charge via www.ccdc.cam.ac.uk/data_request/cif, or by emailing data_request@ccdc.cam.ac.uk, or by contacting The Cambridge Crystallographic Data Centre, 12 Union Road, Cambridge CB2 1EZ, UK; fax: +44 1223 336033.

CCDC 2166695 contains the supplementary crystallographic data for this paper. These data can be obtained free of charge via www.ccdc.cam.ac.uk/data_request/cif, or by emailing data_request@ccdc.cam.ac.uk, or by contacting The Cambridge Crystallographic Data Centre, 12 Union Road, Cambridge CB2 1EZ, UK; fax: +44 1223 336033.

AUTHOR INFORMATION

Corresponding Authors

Li Wang − *Jiangxi Province Key Laboratory of Synthetic Chemistry, School of Chemistry, Biology and Materials Science, East China University of Technology, Nanchang 330013, P. R. China*; Email: wangli20040302@126.com

Feng Luo − *Jiangxi Province Key Laboratory of Synthetic Chemistry, School of Chemistry, Biology and Materials Science, East China University of Technology, Nanchang 330013, P. R. China*; orcid.org/0000-0001-6380-2754; Email: ecitluofeng@163.com

Authors

Wenhui Zhang − *Jiangxi Province Key Laboratory of Synthetic Chemistry, School of Chemistry, Biology and Materials Science, East China University of Technology, Nanchang 330013, P. R. China*

Wansheng Jia − *Jiangxi Province Key Laboratory of Synthetic Chemistry, School of Chemistry, Biology and Materials Science, East China University of Technology, Nanchang 330013, P. R. China*

Jie Qin − *Jiangxi Province Key Laboratory of Synthetic Chemistry, School of Chemistry, Biology and Materials Science, East China University of Technology, Nanchang 330013, P. R. China*

Lan Chen − *Jiangxi Province Key Laboratory of Synthetic Chemistry, School of Chemistry, Biology and Materials Science, East China University of Technology, Nanchang 330013, P. R. China*

Youyuan Ran − *Jiangxi Province Key Laboratory of Synthetic Chemistry, School of Chemistry, Biology and Materials Science, East China University of Technology, Nanchang 330013, P. R. China*

Rajamani Krishna − *Van't Hoff Institute for Molecular Sciences, University of Amsterdam, 1098 XH Amsterdam, The Netherlands*; orcid.org/0000-0002-4784-8530

Complete contact information is available at: https://pubs.acs.org/10.1021/acs.inorgchem.2c01634

Author Contributions

[§]W.Z. and W.J. contributed equally to this work. The manuscript was written through the contributions of all authors.

Notes

The authors declare no competing financial interest.

ACKNOWLEDGMENTS

The authors thank the Open Fund of Jiangxi Province Key Laboratory of Synthetic Chemistry (JXSC202007), Foundation of Jiangxi Educational Committee (GJJ200734), Doctoral Scientific Research Start-up Foundation of East China University of Technology (DHBK2018044), and Provincial College Students Innovation and Entrepreneurship Training Program (S202110405026 and S202110405011).

REFERENCES

(1) Tannert, N.; Sun, Y. Y.; Hastürk, E.; Nießing, S.; Janiak, C. A series of new urea-MOFs obtained via post-synthetic modification of NH_2-MIL-101(Cr): SO_2, CO_2 and H_2O sorption. *Z. Anorg. Allg. Chem.* **2021**, *647*, 1124−1130.

(2) Zhang, Z. H.; Yang, B. L.; Ma, H. P. Aliphatic amine decorating metal−organic framework for durable SO_2 capture from flue gas. *Sep. Purif. Technol.* **2020**, *259*, No. 118164.

(3) Chen, C. Y.; Lu, B.; Zhao, X. F.; Qian, W. Y.; Liu, J.; Trabelsi, T.; Francisco, J. S.; Qin, J.; Li, J.; Wang, L. N.; Zeng, X. Q. Capture of the sulfur monoxide-hydroxyl radical complex. *J. Am. Chem. Soc.* **2020**, *142*, 2175−2179.

(4) Zhang, Y.; Chen, Z. H.; Liu, X.; Dong, Z.; Zhang, P. X.; Wang, J.; Deng, Q.; Zeng, Z. L.; Zhang, S. H.; Deng, S. G. Efficient SO_2 removal using a microporous metal-organic framework with molecular sieving effect. *Ind. Eng. Chem. Res.* **2020**, *59*, 874−882.

(5) Xin, Q. P.; An, K.; Zhang, Y.; Yun, M. Y.; Wang, S. F.; Lin, L. G.; Ye, H.; Ding, X. L.; Li, H.; Zhang, Y. Z. Metal organic frameworks decorated membrane contactor constructing SO_2-philic channels for efficient flue gas desulphurization. *J. Membr. Sci.* **2021**, *620*, No. 118908.

(6) Feng, S. S.; Li, X. Y.; Zhao, S. F.; Hu, Y. X.; Zhong, Z. X.; Xing, W. H.; Wang, H. T. Multifunctional metal organic framework and carbon nanotube-modified filter for combined ultrafine dust capture and SO_2 dynamic adsorption. *Environ. Sci.: Nano* **2018**, *5*, 3023−3031.

(7) Rodríguez-Albelo, L. M.; López-Maya, E.; Hamad, S.; Ruiz-Salvador, A. R.; Calero, S.; Navarro, J. A. R. Selective sulfur dioxide adsorption on crystal defect sites on an isoreticular metal organic framework series. *Nat. Commun.* **2017**, *8*, No. 14457.

(8) López-Olvera, A.; Zárate, J. A.; Martínez-Ahumada, E.; Fan, D.; Díaz-Ramírez, M. L.; Sáenz-Cavazos, P. A.; Martis, V.; Williams, D. R.; Sánchez-González, E.; Maurin, G.; Ibarra, I. A. SO_2 capture by two aluminum-based MOFs: rigid-like MIL-53(Al)-TDC versus breathing MIL-53(Al)-BDC. *ACS Appl. Mater. Interfaces* **2021**, *13*, 39363−39370.

(9) Martínez-Ahumada, E.; Díaz-Ramírez, M. L.; Lara-García, H. A.; Williams, D. R.; Martis, V.; Jancik, V.; Lima, E.; Ibarra, I. A. High and reversible SO_2 capture by a chemically stable Cr(III)-based MOF. *J. Mater. Chem. A* **2020**, *8*, 11515−11520.

(10) Brandt, P.; Xing, S. H.; Liang, J.; Kurt, G.; Nuhnen, A.; Weingart, O.; Janiak, C. Zirconium and aluminum MOFs for low-pressure SO_2 adsorption and potential separation: elucidating the effect of small pores and NH_2 groups. *ACS Appl. Mater. Interfaces* **2021**, *13*, 29137−29149.

(11) Brandt, P.; Nuhnen, A.; Öztürk, S.; Kurt, G.; Liang, J.; Janiak, C. Comparative evaluation of different MOF and non-MOF porous materials for SO_2 adsorption and separation showing the importance of small pore diameters for low-pressure uptake. *Adv. Sustainable Syst.* **2021**, *5*, No. 2000285.

(12) Srivastava, R. K.; Jozewicz, W. Flue gas desulfurization: the state of the art. *J. Air Waste Manage. Assoc.* **2001**, *51*, 1676−1688.

(13) Zhang, Y.; Zhang, P. X.; Yu, W. K.; Zhang, J. H.; Huang, J. J.; Wang, J.; Xu, M.; Deng, Q.; Zeng, Z. L.; Deng, S. G. Highly selective and reversible sulfur dioxide adsorption on a microporous metal−organic framework via polar sites. *ACS Appl. Mater. Interfaces* **2019**, *11*, 10680−10688.

(14) Karousos, D. S.; Vangeli, O. C.; Athanasekou, C. P.; Sapalidis, A. A.; Kouvelos, E. P.; Romanos, G. E.; Kanellopoulos, N. K.

Physically bound and chemically grafted activated carbon supported 1-hexyl-3-methylimidazolium bis(trifluoromethylsulfonyl)imide and 1-ethyl-3-methylimidazolium acetate ionic liquid absorbents for SO_2/CO_2 gas separation. *Chem. Eng. J.* **2016**, *306*, 146−154.
(15) Tchalala, M. R.; Bhatt, P. M.; Chappanda, K. N.; Tavares, S. R.; Adil, K.; Belmabkhout, Y.; Shkurenko, A.; Cadiau, A.; Heymans, N.; Weireld, G. De.; Maurin, G.; Salama, K. N.; Eddaoudi, M. Fluorinated MOF platform for selective removal and sensing of SO_2 from flue gas and air. *Nat. Commun.* **2019**, *10*, No. 1328.
(16) Han, X.; Yang, S. H.; Schrçder, M. Porous metal−organic frameworks as emerging sorbents for clean air. *Nat. Rev. Chem.* **2019**, *3*, 108−118.
(17) Liu, Y.; Bisson, T. M.; Yang, H. Q.; Xu, Z. H. Recent developments in novel sorbents for flue gas clean up. *Fuel Process. Technol.* **2010**, *91*, 1175−1197.
(18) Xing, S.; Liang, J.; Brandt, P.; Schäfer, F.; Nuhnen, A.; Heinen, T.; Boldog, I.; Möllmer, J.; Lange, M.; Weingart, O.; Janiak, C. Capture and separation of SO_2 traces in metal−organic frameworks via pre-synthetic pore environment tailoring by methyl groups. *Angew. Chem., Int. Ed.* **2021**, *60*, 17998−18005.
(19) Zhu, Z. L.; Zhang, P. X.; Li, B.; Chen, S. X.; Deng, Q.; Zeng, Z. L.; Wang, J.; Deng, S. G. Chemical immobilization of amino acids into robust metal−organic framework for efficient SO_2 removal. *AIChE J.* **2021**, *67*, No. e17300.
(20) Suo, X.; Yu, Y.; Qian, S. H.; Zhou, L.; Cui, X. L.; Xing, H. B. Tailoring the pore size and chemistry of ionic ultramicroporous polymers for trace sulfur dioxide capture with high capacity and selectivity. *Angew. Chem., Int. Ed.* **2021**, *60*, 6986−6991.
(21) Goo, J. H.; Irfan, M. F.; Kim, S. D.; Hong, S. C. Effects of NO_2 and SO_2 on selective catalytic reduction of nitrogen oxides by ammonia. *Chemosphere* **2007**, *67*, 718−723.
(22) Ding, S. P.; Liu, F. D.; Shi, X. Y.; Liu, K.; Lian, Z. H.; Xie, L. J.; He, H. Significant promotion effect of Mo additive on a novel Ce−Zr mixed oxide catalyst for the selective catalytic reduction of NO_x with NH_3. *ACS Appl. Mater. Interfaces* **2015**, *7*, 9497−9506.
(23) Smith, G. L.; Eyley, J. E.; Han, X.; Zhang, X.; Li, J. N.; Jacques, N. M.; Godfrey, H. G.; Argent, S. P.; McPherson, L. J. M.; Teat, S. J.; Cheng, Y. Q.; Frogley, M. D.; Cinque, G.; Day, S. J.; Tang, C. C.; Easun, T. L.; Rudić, S.; Ramirez-Cuesta, A. J.; Yang, S. H.; Schröder, M. Reversible coordinative binding and separation of sulfur dioxide in a robust metal−organic framework with open copper sites. *Nat. Mater.* **2019**, *18*, 1358−1365.
(24) Tian, X.-Y.; Zhou, H. L.; Zhang, X. W.; Wang, C.; Qiu, Z. H.; Zhou, D. D.; Zhang, J. P. Two isostructural flexible porous coordination polymers showing contrasting single-component and mixture adsorption properties for propylene/propane. *Inorg. Chem.* **2020**, *59*, 6047−6052.
(25) Wang, X. B.; Zhang, P. X.; Zhang, Z. Q.; Yang, L. F.; Ding, Q.; Cui, X. L.; Wang, J.; Xing, H. B. Efficient separation of propene and propane using anion-pillared metal−organic frameworks. *Ind. Eng. Chem. Res.* **2020**, *59*, 3531−3537.
(26) Fan, W. D.; Wang, X.; Zhang, X. R.; Liu, X. P.; Wang, Y. T.; Kang, Z. X.; Dai, F. N.; Xu, B.; Wang, R. M.; Sun, D. F. Fine-tuning the pore environment of the microporous Cu-MOF for high propylene storage and efficient separation of light hydrocarbons. *ACS Cent. Sci.* **2019**, *5*, 1261−1268.
(27) Yang, L. F.; Cui, X. L.; Yang, Q. W.; Qian, S. H.; Wu, H.; Bao, Z. B.; Zhang, Z. G.; Ren, Q. L.; Zhou, W.; Chen, B. L.; Xing, H. B. A single-molecule propyne trap: highly efficient removal of propyne from propylene with anion-pillared ultramicroporous materials. *Adv. Mater.* **2018**, *30*, No. 1705374.
(28) Yang, L. F.; Cui, X. L.; Zhang, Z. Q.; Yang, Q. W.; Bao, Z. B.; Ren, Q. L.; Xing, H. B. An asymmetric anion-pillared metal-organic framework as a multisite adsorbent enables simultaneous removal of propyne and propadiene from propylene. *Angew. Chem., Int. Ed.* **2018**, *57*, 13145−13149.
(29) Hu, T. L.; Wang, H. L.; Li, B.; Krishna, R.; Wu, H.; Zhou, W.; Zhao, Y. F.; Han, Y.; Wang, X.; Zhu, W. D.; Yao, Z. Z.; Xiang, S. C.; Chen, B. L. Microporous metal-organic framework with dual functionalities for highly efficient removal of acetylene from ethylene/acetylene mixtures. *Nat. Commun.* **2015**, *6*, No. 7328.
(30) Li, H.; Li, L. B.; Lin, R. B.; Ramirez, G.; Zhou, W.; Krishna, R.; Zhang, Z. J.; Xiang, S. H.; Chen, B. L. Microporous metal-organic framework with dual functionalities for efficient separation of acetylene from light hydrocarbon mixtures. *ACS Sustainable Chem. Eng.* **2019**, *7*, 4897−4902.
(31) Li, B. Y.; Zhang, Y. M.; Krishna, R.; Yao, K. X.; Han, Y.; Wu, Z. L.; Ma, D. X.; Shi, Z.; Pham, T.; Space, B.; Liu, J.; Thallapally, P. K.; Liu, J.; Chrzanowski, M.; Ma, S. Q. Introduction of π-complexation into porous aromatic framework for highly selective adsorption of ethylene over ethane. *J. Am. Chem. Soc.* **2014**, *136*, 8654−8660.
(32) Yang, S. H.; Ramirez-Cuesta, A. J.; Newby, R.; Garcia-Sakai, V.; Manuel, P.; Callear, S. K.; Campbell, S. I.; Tang, C. C.; Schröder, M. Supramolecular binding and separation of hydrocarbons within a functionalized porous metal−organic framework. *Nat. Chem.* **2015**, *7*, 121−129.
(33) Zhang, Z. Q.; Peh, S. B.; Krishna, R.; Kang, C. J.; Chai, K. G.; Wang, Y. X.; Shi, D. C.; Zhao, D. Optimal pore chemistry in an ultramicroporous metal−organic framework for benchmark inverse CO_2/C_2H_2 separation. *Angew. Chem., Int. Ed.* **2021**, *60*, 17198−17204.
(34) Fan, W. D.; Yuan, S.; Wang, W. J.; Feng, L.; Liu, X. P.; Zhang, X. R.; Wang, X.; Kang, Z. X.; Dai, F. N.; Yuan, D. Q.; Sun, D. F.; Zhou, H. C. Optimizing multivariate metal-organic frameworks for efficient C_2H_2/CO_2 separation. *J. Am. Chem. Soc.* **2020**, *142*, 8728−8737.
(35) Zhang, Y. B.; Yang, L. F.; Wang, L. Y.; Cui, X. L.; Xing, H. B. Pillar iodination in functional boron cage hybrid supramolecular frameworks for high performance separation of light hydrocarbons. *J. Mater. Chem. A* **2019**, *7*, 27560−27566.
(36) Xu, Z. Z.; Xiong, X. H.; Xiong, J. B.; Krishna, R.; Li, L. B.; Fan, Y. L.; Luo, F.; Chen, B. L. A robust Th-azole framework for highly efficient purification of C_2H_4 from a $C_2H_4/C_2H_2/C_2H_6$ mixture. *Nat. Commun.* **2020**, *11*, No. 3163.
(37) Savage, M.; Cheng, Y. Q.; Easun, T. L.; Eyley, J. E.; Argent, S. P.; Warren, M. R.; Lewis, W.; Murray, C.; Tang, C. C.; Frogley, M. D.; Cinque, G.; Sun, J. L.; Rudić, S.; Murden, R. T.; Benham, M. J.; Fitch, A. N.; Blake, A. J.; Ramirez-Cuesta, A. J.; Yang, S. H.; Schröder, M. Selective adsorption of sulfur dioxide in a robust metal−organic framework material. *Adv. Mater.* **2016**, *28*, 8705−8711.
(38) Brandt, P.; Nuhnen, A.; Lange, M.; Möllmer, J.; Weingart, O.; Janiak, C. Metal-organic frameworks with potential application for SO_2 separation and flue gas desulfurization. *ACS Appl. Mater. Interfaces* **2019**, *11*, 17350−17358.
(39) Mounfield, W. P.; Han, C.; Pang, S. H.; Tumuluri, U.; Jiao, Y.; Bhattacharyya, S.; Dutzer, M. R.; Nair, S.; Wu, Z.; Lively, R. P.; Sholl, D. S.; Walton, K. S. Synergistic effects of water and SO_2 on degradation of MIL-125 in the presence of acid gases. *J. Phys. Chem. C* **2016**, *120*, 27230−27240.
(40) Yang, S. H.; Liu, L. F.; Sun, J. L.; Thomas, K. M.; Davies, A. J.; George, M. W.; Blake, A. J.; Hill, A. H.; Fitch, A. N.; Tang, C. C.; Schröder, M. Irreversible network transformation in a dynamic porous host catalyzed by sulfur dioxide. *J. Am. Chem. Soc.* **2013**, *135*, 4954−4957.
(41) Andreo, J.; Priola, E.; Alberto, G.; Benzi, P.; Marabello, D.; Proserpio, D. M.; Lamberti, C.; Diana, E. Autoluminescent Metal−Organic Frameworks (MOFs): Self-Photoemission of a Highly Stable Thorium MOF. *J. Am. Chem. Soc.* **2018**, *140*, 14144−14149.
(42) Li, Y.; Weng, Z.; Wang, Y.; Chen, L.; Sheng, D.; Liu, Y.; Diwu, J.; Chai, Z.; Albrecht-Schmitt, T. E.; Wang, S. Centrosymmetric and Chiral Porous Thorium Organic Frameworks Exhibiting Uncommon Thorium Coordination Environments. *Dalton Trans.* **2015**, *44*, 20867−20873.
(43) Chen, F. Q.; Lai, D.; Guo, L. D.; Wang, J.; Zhang, P. X.; Wu, K. Y.; Zhang, Z. G.; Yang, Q. W.; Yang, Y. W.; Chen, B. L.; Ren, Q. L.; Bao, Z. B. Deep desulfurization with record SO_2 adsorption on the metal-organic frameworks. *J. Am. Chem. Soc.* **2021**, *143*, 9040−9047.

https://doi.org/10.1021/acs.inorgchem.2c01634
Inorg. Chem. 2022, 61, 11879−11885

(44) Fan, Y. L.; Zhang, H. P.; Yin, M. J.; Krishna, R.; Feng, X. F.; Wang, L.; Luo, M. B.; Luo, F. High adsorption capacity and selectivity of SO_2 over CO_2 in a metal-organic framework. *Inorg. Chem.* **2021**, *60*, 4−8.
(45) Cui, X.; Yang, Q. W.; Yang, L. F.; Krishna, R.; Zhang, Z. G.; Bao, Z. B.; Wu, H.; Ren, Q. L.; Zhou, W.; Chen, B. L.; Xing, H. B. Ultrahigh and selective SO_2 uptake in inorganic anion-pillared hybrid porous materials. *Adv. Mater.* **2017**, *29*, No. 1606929.
(46) Britt, D.; Tranchemontagne, D.; Yaghi, O. M. Metal-organic frameworks with high capacity and selectivity for harmful gases. *Proc. Natl. Acad. Sci. U.S.A.* **2008**, *105*, 11623−11627.
(47) Wang, L.; Yang, L.; Gong, L.; Krishna, R.; Gao, Z.; Tao, Y.; Yin, W.; Xu, Z.; Luo, F. Constructing redox-active microporous hydrogen-bonded organic framework by imide-functionalization: electrochromism, and selective adsorption of C_2H_2 over CO_2. *Chem. Eng. J.* **2020**, *383*, No. 123117.
(48) Matsuda, R.; Kitaura, R.; Kitagawa, S.; Kubota, Y.; Belosludov, R. V.; Kobayashi, T. C.; Sakamoto, H.; Chiba, T.; Takata, M.; Kawazoe, Y.; Mita, Y. Highly controlled acetylene accommodation in a Metal−Organic microporous material. *Nature* **2005**, *436*, 238−241.
(49) Zhang, H.; Fan, Y.; Krishna, R.; Feng, X.; Wang, L.; Luo, F. Robust metal−organic framework with multiple traps for trace Xe/Kr separation. *Sci. Bull.* **2021**, *66*, 1073−1079.
(50) Yumitori, S. Correlation of C1s chemical state intensities with the O1s intensity in the XPS analysis of anodically oxidized glasslike carbon samples. *J. Mater. Sci.* **2000**, *35*, 139−146.
(51) Zhang, J. H.; Zhang, P. X.; Li, M. Y.; Shan, Z. W.; Wang, J.; Deng, Q.; Zeng, Z. L.; Deng, S. G. Facile preparation of biomass-derived mesoporous carbons for highly efficient and selective SO_2 capture. *Ind. Eng. Chem. Res.* **2019**, *58*, 14929−14937.

https://doi.org/10.1021/acs.inorgchem.2c01634
Inorg. Chem. 2022, 61, 11879−11885

Efficient separation of trace SO_2 from $SO_2/CO_2/N_2$ mixtures in a Th-based MOF

*Wenhui Zhang[†a], Wansheng Jia[†a], Jie Qin[a], Lan Chen[a], Youyuan Ran[a], Rajamani Krishna[b], Li Wang[*a], and Feng Luo[*a]*

[a] Jiangxi Province Key Laboratory of Synthetic Chemistry, School of Chemistry, Biology and Materials Science, East China University of Technology, Nanchang 330013, P. R. China

[b] Van't Hoff Institute for Molecular Sciences, University of Amsterdam, Science Park 904, 1098 XH Amsterdam, The Netherlands

† These authors contributed equally to this work

E-mail: wangli20040302@126.com ecitluofeng@163.com

Experimental Methods

Materials:

Caution! $Th(NO_3)_4$ used in this study is a radioactive and chemically toxic reactant, so standard precautions and protection for handling such substances have been followed.

The ligand 1,3,6,8-tetrakis (P-benzoic acid) pyrene (H_4TBAPy) was purchased from EXTENSION Technology Co.,Ltd. Other materials such as $Th(NO_3)_4$, N, N-dimethylformamide (DMF), and Trifluoroacetic acid (TFA) were purchased from Aladdin Chemistry Co., Ltd. without further purification.

Synthesis of ECUT-Th-60

ECUT-Th-60 was prepared by solvothermal method. Specifically, $Th(NO_3)_4$ (12 mg) and ligand H_4TBAPy (17 mg) were mixed in 3.0 mL N, N-dimethylformamide (DMF) solution. About 300 μL TFA was added in the mixture. Then the mixture was placed into reactor and the temperature was set for 150^{o}C. After three days, the reactor was cooled down to room temperature and yellow crystals were obtained.

Synthesis of activated ECUT-Th-60 (ECUT-Th-60a)

Bulk **ECUT-Th-60** was immersed into methanol for three days. The methanol was changed three times every day. Subsequently, **ECUT-Th-60** was activated at 150^{o}C overnight under vacuum conditions to obtain **ECUT-Th-60a**.

Physical Measurements

The X-ray diffraction data of single crystal was collected at 298 K on a Bruker-Appex (II) diffractometer using graphite monochromated MoKα radiation (λ=0.71073 Å). The data of X-ray powder diffraction were collected on a Bruker AXSD8 Discover powder diffractometer at 40 kV/40 mA for Cu Kα (λ= 1.5406 Å) at room temperature in the range of 5-50 °(2θ) with a scan speed of 0.1 °per step. Thermogravimetric analysis (TG) was performed by a TGA Q500 thermal analysis system. All TGA experiments were performed under air condition from room temperature to 800°C at a rate of 5°C/min.

Gas adsorption experiments.

The gas sorption isotherms were collected on a Belsorp-max. Roughly 100 mg of **ECUT-Th-60** were taken for the nitrogen adsorption experiments at 77 K. The adsorption isotherms for SO_2 and CO_2 were obtained at temperature of 273 K and 298 K, respectively. Liquid nitrogen and water bath were used to maintain the experimental temperatures of 77 K, 273 K, and 298 K.

Fitting of experimental data on pure component isotherms

The unary isotherm data for SO_2 in **ECUT-Th-60** at 273 K, and 298 K were fitted with the dual-site Langmuir model, where we distinguish two distinct adsorption sites A and B:

$$q = \frac{q_{sat,A} b_A p}{1 + b_A p} + \frac{q_{sat,B} b_B p}{1 + b_B p} \tag{S1}$$

with T-dependent parameters b_A, and b_B

$$b_A = b_{A0} \exp\left(\frac{E_A}{RT}\right); \quad b_B = b_{B0} \exp\left(\frac{E_B}{RT}\right) \tag{S2}$$

The unary isotherm data for CO_2, and N_2 in **ECUT-Th-60** at 273 K, and 298 K are fitted with good accuracy using the 1-site Langmuir model, with T-dependent parameters b_A.

The unary isotherm fit parameters for SO_2, CO_2, and N_2 are provided in Table S1.

Table S1. Dual-site Langmuir parameter fits for SO_2, CO_2, and N_2 in **ECUT-Th-60**.

	Site A			Site B		
	$q_{A,sat}$ mol kg^{-1}	b_A Pa^{-1}	E_A kJ mol^{-1}	$q_{B,sat}$ mol kg^{-1}	b_B Pa^{-1}	E_B kJ mol^{-1}
SO_2	3	1.458E-06	13	1	2.008E-16	60
CO_2	3.5	6.201E-09	17.8			
N_2	0.32	8.470E-06	1			

Calculation of Isosteric Heat of Adsorption

The isosteric heats of adsorption were calculated from the dual-site Langmuir-Freundlich isotherms for **ECUT-Th-10a** using

$$Q_{st} = RT^2 \left(\frac{\partial \ln p}{\partial T} \right)_q \quad \text{(S3)}$$

Where p is the pressure, T is the temperature, R is the gas constant (8.314 J mol^{-1} K^{-1}). By drawing the ln$P$ vs 1/T plot of gas at various loading, Q_{st} = -slope×R.

Calculation of selectivity via ideal adsorption solution theory (IAST)

The adsorption selectivity of SO_2/CO_2 (1/99) and SO_2 /N_2 (1/99) in **ECUT-Th-60** and was established by the Ideal Adsorbed Solution Theory (IAST). The adsorption selectivity was calculated from

$$S_{ads} = \frac{q_A / q_B}{y_A / y_B} \quad \text{(S4)}$$

where the q_A, and q_B represent the molar loadings in **ECUT-Th-60** that is in equilibrium with a bulk fluid mixture with mole fractions y_A, and y_B = 1 - y_A. The molar loadings, also called *gravimetric uptake capacities*, are expressed in mol kg^{-1}.

Transient breakthrough simulations

The performance of industrial fixed bed adsorbers is dictated by a combination of adsorption selectivity and uptake capacity. Transient breakthrough simulations were carried out using the methodology described in earlier publications.[1-5] The mixtures (1/99 SO_2/CO_2 mixtures at 298 K and 100 kPa) were investigated.

For the breakthrough simulations, the following parameter values were used: length of packed bed, L = 0.3 m; voidage of packed bed, ε = 0.4; superficial gas velocity at inlet, u = 0.04 m/s.

The *y*-axis is the dimensionless concentrations of each component at the exit of the fixed bed, c_i/c_{i0} normalized with respect to the inlet feed concentrations. The *x*-axis is the *dimensionless* time, $\tau = \frac{tu}{L\varepsilon}$, defined by dividing the actual time, *t*, by the characteristic time, $\frac{L\varepsilon}{u}$.

L	length of packed bed adsorber, m
t	time, s
T	absolute temperature, K
u	superficial gas velocity in packed bed, m s^{-1}
ε	voidage of packed bed, dimensionless
τ	time, dimensionless

Breakthrough experiments.

The breakthrough experiments were performed at 298 K. Bulk powder **ECUT-Th-60a** (around 800 mg) were filled into stainless steel column (Φ 46 mm×150 mm). First, the helium gas (100 mL/min) was introduced into the column for 30 min. Then the different gas mixture SO_2/CO_2 (containing 2000 ppm SO_2) and $SO_2/CO_2/N_2$ mixture with or without water were passed through the column with 10 mL/min. The eluted gas stream from the column is monitored by a Hiden mass-spectrometer. Prior to each cycling experiment, the adsorption bed was regenerated by He flow for 3h at 333 K to ensure complete removal of adsorbed gas.

Table S2. Crystal structure information for **ECUT-Th-60**.

Compound	**ECUT-Th-60**
Formula	$C_{88}H_{36}O_{24}Th_3$
Formula weight	2173.33
Color	Yellow

Crystal system	monoclinic
Space group	*C2/m*
a(Å)	32.6642(16)
b(Å)	29.7904(16)
C (Å)	11.7665(6)
α	90
β	92.590(4)
γ	90
Volume (Å^3)	11438.1(10)
Z	4
Temperature for data collection (K)	293
Range for data collection θ(°)	3.319 to 25
No. of measured reflections	10248
No. of parameters	468
Goodness-of-fit on F2	1.082
Final R indexes[I≥2σ(I)]	R_1=0.1560,wR_2=0.4066
Final R indexes [all data]	R_1=0.2094,wR_2=0.4384

$R_1 = \Sigma||F_o|-|F_c||/\Sigma|F_o|$. $wR_2 = [\Sigma w (F_o^2-F_c^2)^2/\Sigma w (F_o^2)^2]^{1/2}$.

Table S3 Selected bond length (Å) and angles (°)for **ECUT-Th-60**

Bond length

Th(1)-O(1)#2	2.439(19)	Th(1)-O(2)	2.269(9)
Th(1)-O(7)#2	2.47(2)	Th(1)-O(8)	2.49(2)
Th1(1)-O(9)	2.55(5)	Th(1)-O(10)#3	2.48(2)
Th(1)-O(3)	2.398(17)	Th(1)-O(11)	2.528(16)
Th(2)-O(2)	2.360(16)	Th(2)-O(2) #3	2.360(16)

Th(2)-O(4)#4	2.43(2)	Th(2)-O(4) #2	2.43(2)
Th1(2)-O(5)#3	2.38(2)	Th(2)-O(5)	2.38(2)
Th(2)-O(12)	2.37(2)	Th(2)-O(12) #3	2.37(2)
Th(2)-O(13)	2.74(5)	Th(2)-O(13) #3	2.74(5)

Symmetrical code: [1]-X,+Y,-1-Z; [2]1/2-X,3/2-Y,-Z; [3]-X,+Y,-Z; [4]-1/2+X,3/2-Y,+Z; [5]+X,1-Y,+Z

Bond angles

O(1)#1-Th(1)-O(7)#1	72.3(6)	O(1)-Th(1)-O(8)	70.2(8)
O(1)#1-Th(1)-O(9)	95.3(11)	O(1)#1-Th(1) -O(10)#3	135.4(9)
O(1)#1-Th(1)-O(11)	75.0(9)	O(2)-Th(1)-O(1)#1	140.6 (6)
O(2)-Th(1)-O(7) #1	68.4(6)	O(2)-Th(1)-O(8)	95.7(7)
O(2)-Th(1)-O(9)	72.2(10)	O(2)-Th(1)-O(10)#3	70.6(7)
O(2)-Th(1)-O(3)	137.3(8)	O(2)-Th(1)-O(11)	140.2(9)
O(7)#1-Th(1)-O(8)	72.1(9)	O(7)#1-Th(1)-O(9)	68.6(10)
O(7)#1-Th(1)-O(10)#3	124.9(7)	O(7)#1-Th(1)-O(11)	142.1
O(8)-Th(1)-O(9)	140.6 (10)	O(8)-Th(1)-O(9)	140.6(10)
O(8)-Th(1)-O(11)	79.4(8)	O(10)#3-Th(1)-O(8)	77.1(10)
O(10)#3-Th(1)-O(9)	128.8(12)	O(3)-Th(1)-O(1)#1	59.6(8)
O(3)-Th(1)-O(7)#1	109.2(7)	O(3)-Th(1)-O(8)	125.1(8)
O(3)-Th(1)-O(9)	68.0(10)	O(3)-Th(1)-O(10)#3	125.8(7)
O(3)-Th(1)-O(11)	68.1(6)	O(11)-Th(1)-O(9)	133.6(9)
O(2)-Th(2)-O(2)#3	97.8(8)	O(2) #3-Th(2)-O(4)#4	67.5(6)
O(2)#3-Th(2)-O(4)#1	69.9(6)	O(2) -Th(2)-O(4)#1	67.5(6)
O(2)-Th(2)-O(4)#4	69.9(6)	O(2) -Th(2)-O(5)#3	75.7(7)
O(2)#3-Th(2)-O(5)#3	145.3(7)	O(2) -Th(2)-O(5)	145.3(7)
O(2)#3-Th(2)-O(5)	75.7(7)	O(2) -Th(2)-O(12)	80.5(6)
O(2)#3-Th(2)-O(12)	142.2(7)	O(2) -Th(2)-O(12)#3	142.2(7)
O(2)#3-Th(2)-O(12)#3	80.5(6)	O(2)#3-Th(2)-O(13)#3	130.5(14)
O(2)-Th(2)-O(13)#3	130.5(14)	O(2) -Th(2)-O(13)	130.5(14)
O(2)-Th(2)-O(13)#3	130.9 (15)	O(2) -Th(2)-O(13)#3	130.9(15)
O(2)#3-Th(2)-O(13)	130.5(14))	O(4) #1-Th(2)-O(4)#4	112.9(12)
O(4)#1-Th(2)-O(13)	116.4(12)	O(4) #4-Th(2)-O(13)#3	116.4(12)
O(4)#1-Th(2)-O(13)#3	130.7(12)	O(4) #4-Th(2)-O(13)	130.7(12)
O(5)#3-Th(2)-O(4)#4	78.5(8)	O(5) #3-Th(2)-O(4)#1	133.1(5)
O(5)-Th(2)-O(4)#4	133.1(5)	O(5) #1-Th(2)-O(4)#1	78.5(8)
O(5)#3-Th(2)-O(5)	128.1(12)	O(5) -Th(2)-O(13)#3	68.4(1)
O(5)#3-Th(2)-O(13)#3	60.0 (14)	O(5)-Th(2)-O(13)	60.4(14)
O(5)#3-Th(2)-O(13)	68.4(14)	O(12)#3-Th(2)-O(4)#4	74.7(8)
O(12)-Th(2)-O(4)#4	142.0(6)	O(12)#3-Th(2)-O(4)#1	142.0(6)
O(12)-Th(2)-O(4)#1	74.7(8)	O(12)#3-Th(2)-O(5)#3	84.5(6)
O(12)#3-Th(2)-O(5)#3	71.4(8)	O(12)#3-Th(2)-O(5)	71.4(8)
O(12)-Th(2)-O(5)	84.5 (6)	O(12)-Th(2)-O(12)3	123.3(12)
O(12)#3-Th(2)-O(13)	66.8(14)	O(12)-Th(2)-O(13)#3	66.8(14)
O(12)#3-Th(2)-O(13)#3	56.7(14)	O(12)-Th(2)-O(13)	56.7(14)

Symmetrical code: [1]1/2-X,3/2-Y,-Z; [2]-X,+Y,-1-Z; [3]-X,+Y,-Z; [4]-1/2+X,3/2-Y,+Z; [5]+X,1-Y,+Z

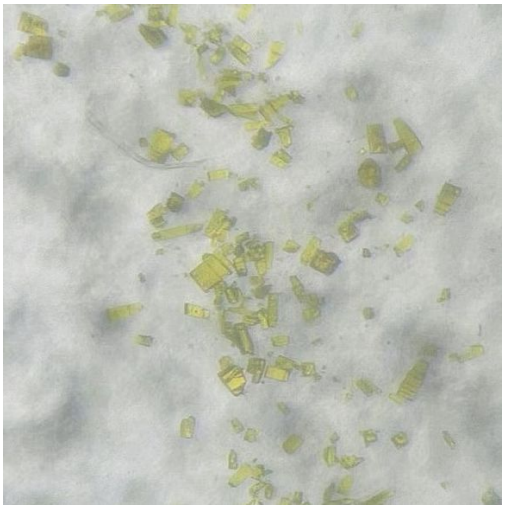

Figure S1. The photograph of **ECUT-Th-60**

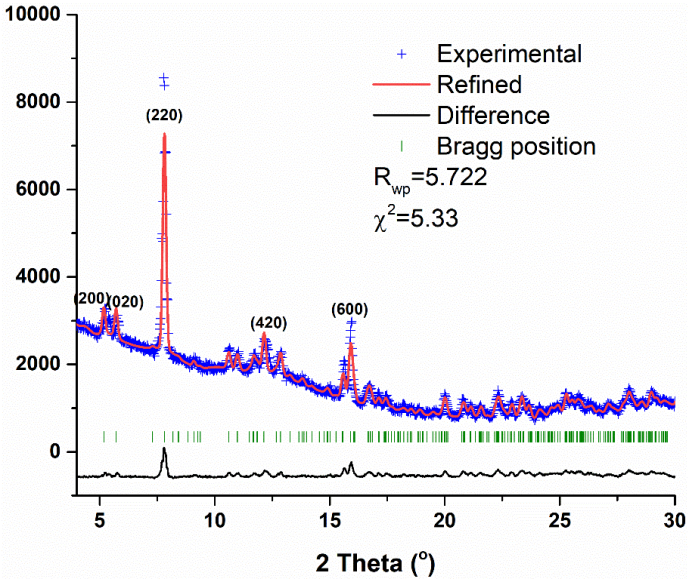

Figure S2. The Rietveld refinement performed on X-ray powder diffraction data of **ECUT-Th-60**.

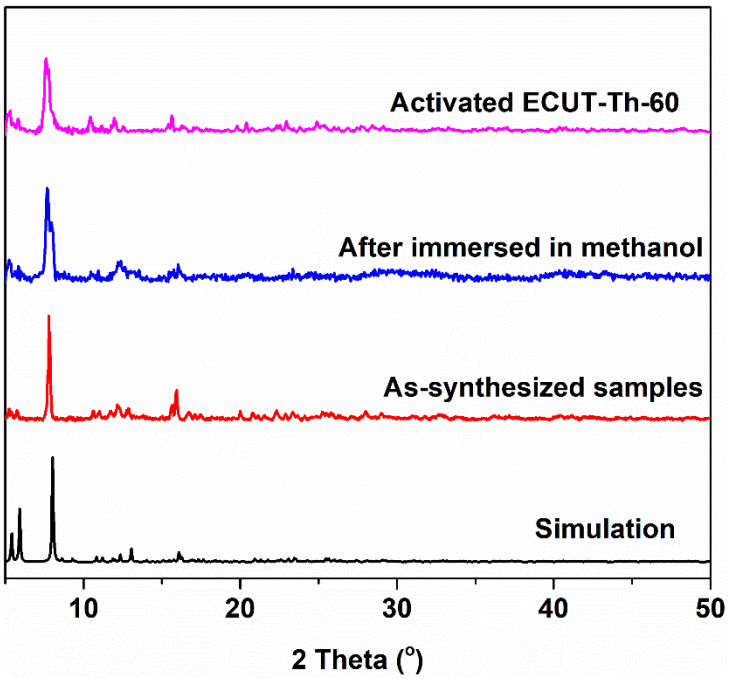

Figure S3. The PXRD patterns of the simulated data and the as-synthesized samples.

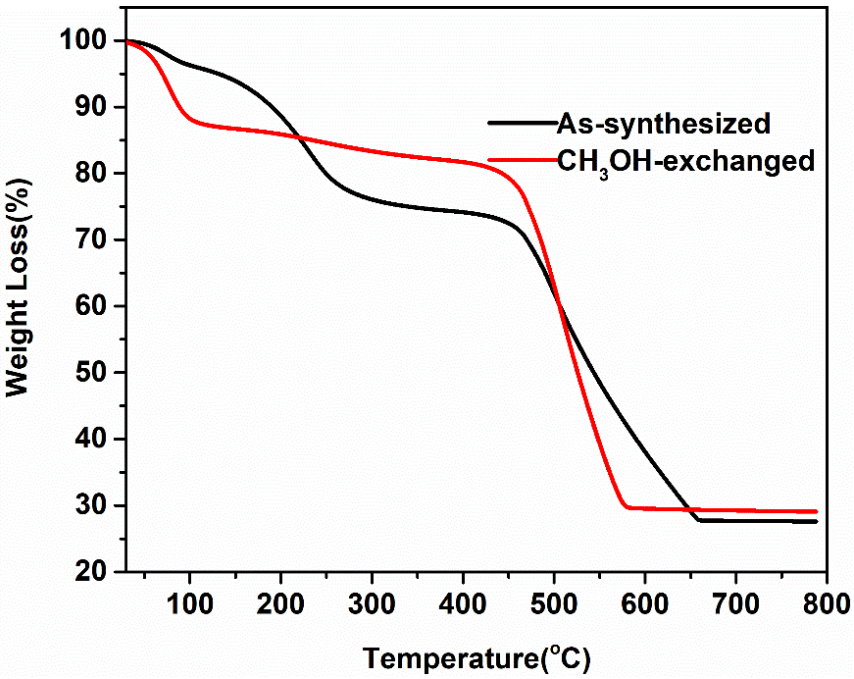

Figure S4. The TG curves of **ECUT-Th-60** (black) and the CH_3OH-exchanged samples (red).

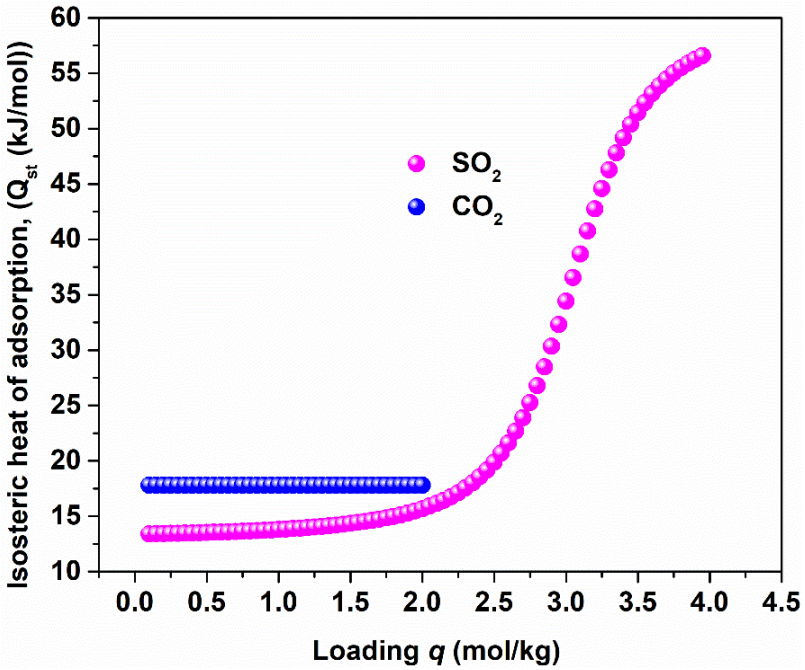

Figure S5. The Q_{st} value of SO_2 and CO_2 for **ECUT-Th-60**.

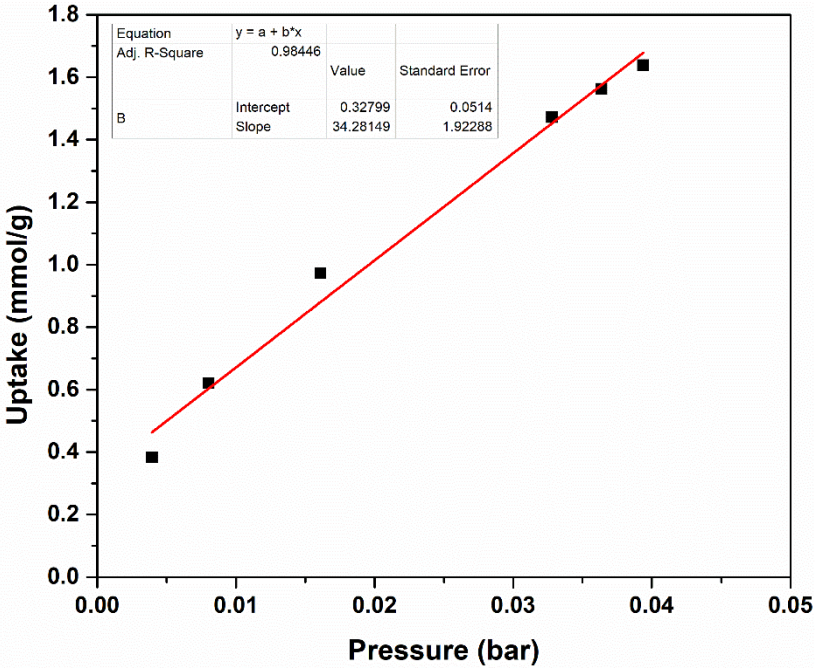

Figure S6. The Henry fitting of SO_2 adsorption on **ECUT-Th-60**.

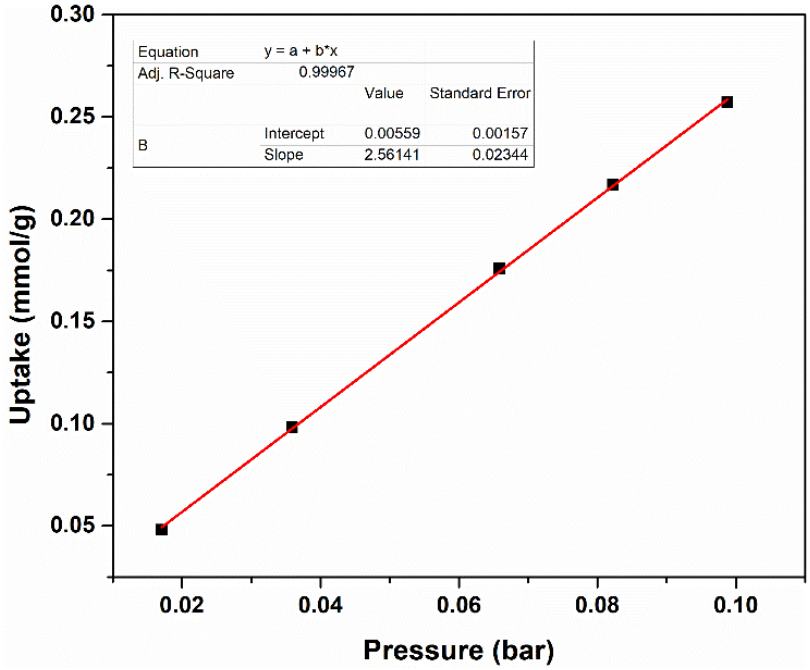

Figure S7. The Henry fitting of SO_2 adsorption on **ECUT-Th-60**.

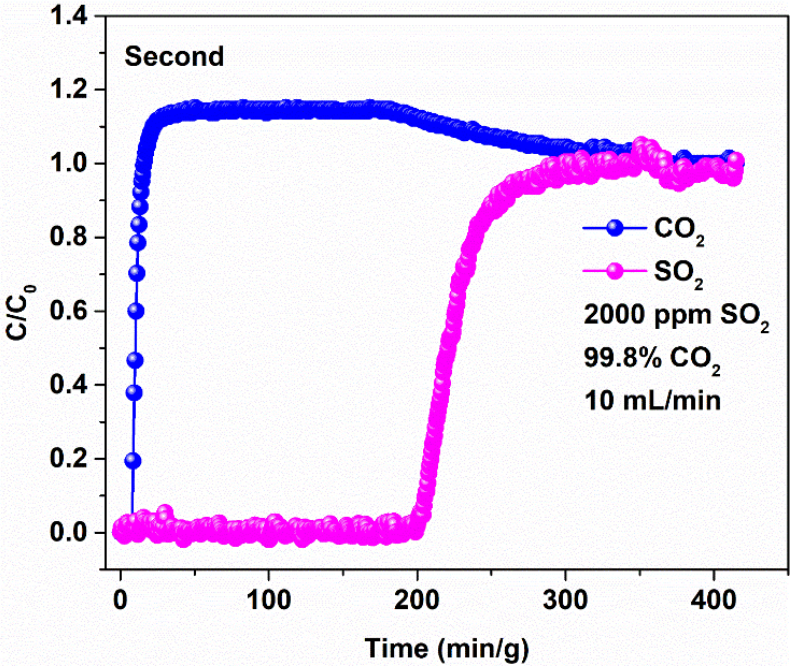

Figure S8. The second experimental breakthrough curve of **ECUT-Th-60** for SO_2/CO_2 mixture.

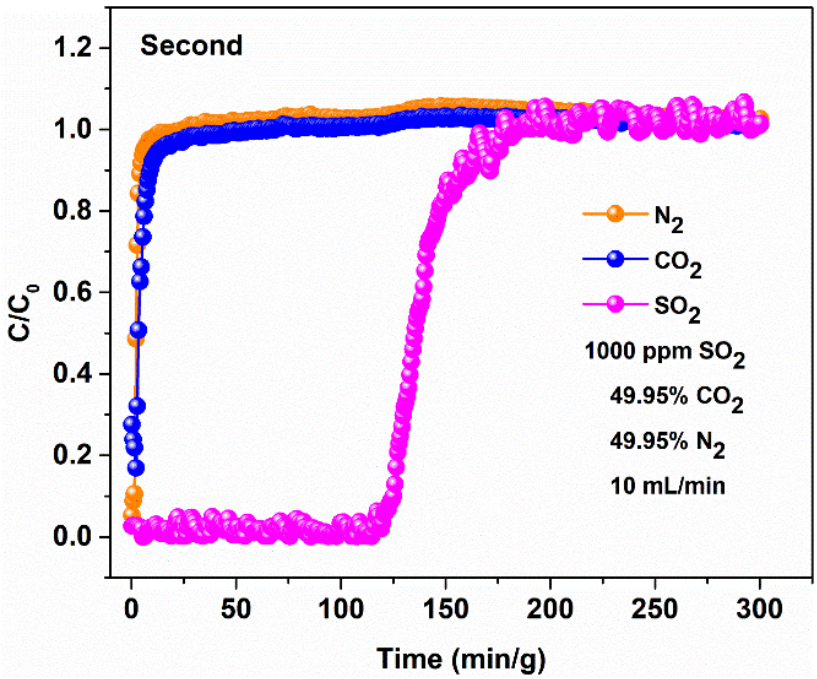

Figure S9. The second experimental breakthrough curve of **ECUT-Th-60** for a $SO_2/CO_2/N_2$ mixture without water.

References:

(1) Krishna, R. The Maxwell-Stefan Description of Mixture Diffusion in Nanoporous Crystalline Materials. Microporous Mesoporous Mater. 2014, 185, 30-50.

(2) Krishna, R. Methodologies for Evaluation of Metal-Organic Frameworks in Separation Applications. RSC Adv. 2015, 5, 52269-52295.

(3) Krishna, R. Screening Metal-Organic Frameworks for Mixture Separations in Fixed-Bed Adsorbers using a Combined Selectivity/Capacity Metric. RSC Adv. 2017, 7, 35724-35737.

(4) Krishna, R. Methodologies for Screening and Selection of Crystalline Microporous Materials in Mixture Separations. Sep. Purif. Technol. 2018, 194, 281-300.

(5) Krishna, R. Metrics for Evaluation and Screening of Metal-Organic Frameworks for Applications in Mixture Separations. ACS Omega 2020, 5, 16987−17004.